Evaluation of different oxygen carriers for biomass tar reforming

1: Carbon deposition in experiments with toluene

Mendiara, Teresa; Johansen, Joakim Myung; Utrilla, Rubén; Geraldo, Paulo; Jensen, Anker Degn; Glarborg, Peter

Published in:
Fuel

Link to article, DOI:
10.1016/j.fuel.2010.11.028

Publication date:
2011

Evaluation of different oxygen carriers for biomass tar reforming (I): carbon deposition in experiments with toluene

Teresa Mendiara [a,*], Joakim M. Johansen [b], Rubén Utrilla [a], Paulo Geraldo [b], Anker D. Jensen [b] and Peter Glarborg [b]

[a] *Department of Energy and Environment, Instituto de Carboquímica (CSIC), Miguel Luesma Castán 4, 50018 Zaragoza, Spain*

[b] *Department of Chemical and Biochemical Engineering, Technical University of Denmark, 2800 Lyngby, Denmark*

Abstract

In this work, an innovative method for gas conditioning in biomass gasification is analyzed. The objective is to remove tar by selectively reforming the unwanted hydrocarbons in the product gas with a Chemical Looping Reformer (CLR), while minimizing the carbon formation during the process. Toluene, in a concentration of 600-2000 ppmv, was chosen as a tar model compound. Experiments were performed in a TGA apparatus and a fixed bed reactor. Four oxygen carriers (60% NiO / $MgAl_2O_4$ (Ni60), 40% NiO / $NiAl_2O_4$ (Ni40), 40% Mn_3O_4 / Mg-ZrO_2 (Mn40) and $FeTiO_3$ (Fe)) were tested under alternating reducing/oxidizing cycles. Several variables affecting the reducing cycle were analyzed: temperature, time for the reduction step and H_2O/C_7H_8 molar ratio. Ni40 and Mn40 presented interesting characteristics for CLR of biomass tar. Both showed stable reactivity to C_7H_8 after a few cycles. Ni40 showed a high tendency to carbon deposition compared to Mn40, spe-

cially at high temperatures. Carbon deposition could be controlled by decreasing the temperature and the time for the reduction step. The addition of water also reduced the amount of carbon deposited, which was completely avoided working with a H_2O/C_7H_8 molar ratio of 26.4.

Key words: biomass gasification, chemical looping, reforming, tar, toluene

1 Introduction

Biomass gasification is considered as a promising technology for energy production. One of the main drawbacks still remaining for its breakthrough is the formation of tar during the process and the subsequent upgrading of the biomass gas [1]. The main problem with tar is that it easily condenses [2], causing fouling and therefore seriously affecting the operation of the process. Tar formation is highly dependent on the gasification conditions. When biomass is pyrolyzed at high temperature, secondary reactions occur in the gas phase which convert oxygenated tar compounds to light hydrocarbons, aromatics, oxygenates and olefins, subsequently forming higher hydrocarbons and larger PAH in tertiary processes [3]. The presence of oxygen and steam can influence the cracking of these products and determine the final composition of the tar produced [4–7].

During the past years several gas cleaning technologies for tar removal have been used. Among them, hot gas conditioning by catalytic reforming has proven to be the best solution for mitigating biomass gasification tars. Differ-

* Corresponding author
Email address: tmendiara@icb.csic.es
Phone: +34 976 733 977
Fax: +34 976 733 318 (Teresa Mendiara).

ent catalysts have been tested, but Ni-based became the most widely used [8]. Ni-based catalysts present high effectiveness for tar conversion, although several factors may lead to their rapid deactivation, such as catalyst poisoning by sulfur, chlorine or alkali metals, and coke formation, which normally is considered as the main problem.

In the reforming process, the carbon species can either react with water to form gaseous products (H_2, CO and CO_2) or go through a series of steps leading to carbon deposition [9]:

$$2\,CO \overset{surf}{\rightleftharpoons} C(s) + CO_2 \tag{1}$$

$$CO + H_2 \overset{surf}{\rightleftharpoons} C(s) + H_2O \tag{2}$$

$$C_nH_{2n+2} \overset{surf}{\rightleftharpoons} n\,C(s) + (n+1)\,H_2 \tag{3}$$

The formation of coke through reactions (1) (Boudouard reaction) and (2) is favoured at temperatures lower than 650 °C [10], but formation via reaction (3) becomes increasingly important at higher temperatures. In the case of high hydrocarbons (tars), reaction (3) can be considered irreversible [11]. The tendency of carbon to deposit depends on the nature of the surface carbon species. Previous steam reforming studies have indicated that the more unsaturated the hydrocarbon, the more extensive the carbon deposition [12].

The present study aims to contribute to the development of innovative and efficient technologies for biomass tar cleaning. More specifically, this study is focused on the so-called Chemical Looping technology. This technology was first applied to combustion processes with CO_2 capture [13–16]. Chemical Looping Combustion (CLC) uses two separate reactors, one for air and one

for fuel. A solid carrier, normally a metal oxide (M_xO_y), transports the oxygen between the reactors, therefore avoiding direct contact between fuel and air. The same basic principles are present in Chemical Looping Reforming (CLR) (Figure 1). The main difference is that CLR is not intended for heat production but designed for partial oxidation and steam reforming of hydrocarbon fuels, so the wanted products are H_2 and CO. The CLR technology offers a method to clean the tars in a way that will both preserve energy and prevent clogging. The CLR operates at a temperature well above the condensation point of the tars. The raw gas from the gasifier will need no heating prior to the CLR. Although catalytic reforming can also be done in the same temperature range as the gasification, it presents as drawback that catalysts are sensitive to poisoning by carbon deposition. In the CLR, the heavier organic components of the raw gas will be oxidized/reformed by circulating oxygen carriers in the form of metal oxides. The spent metal oxides will be recirculated to the air reactor, where carbon deposited will be combusted and the metal oxides reoxidized.

For many years, the development of oxygen carriers adequate for CL processes has been the focus of study. Heterogeneous catalysts used for hydrocarbon reforming were the starting point. However, in CLC and CLR the oxygen carrier acts as a source of undiluted oxygen. The solid circulation rate depends on the oxygen carrier capacity of the carriers, therefore higher ratios of active material (20-80%) were used, as compared to the heterogeneous catalysts (less than 10%). Transition metal oxides such as nickel, copper, cobalt, iron and manganese on different supports such as SiO_2, TiO_2, ZrO_2 or yttria-stabilized ZrO_2 (YSZ), Al_2O_3 and bentonite have been tested [16, 17], as well as novel materials such as perovskites [18].

Regarding CLR, most of the studies performed until now analyze CH_4 reforming to obtain H_2 using NiO/Ni as oxygen carrier. NiO/Ni appears to be an interesting material, not only due to its high reactivity, but also for its selectivity to H_2 and CO and the reforming activity once NiO is reduced to Ni [19–21]. Materials like Fe_2O_3 and Mn_3O_4, despite being cheaper and environmentally friendly, are reduced to new oxide phases rather than to metals and therefore have shown less reactivity with CH_4 [19].

Formation of solid carbon has also been identified as a potential problem in CLR of methane [22, 23]. Some studies have analyzed the effect of different operating conditions on the carbon deposition. In the 800-950 °C temperature range, de Diego et al. [24], working with a Ni-based oxygen carrier, found that both the carrier conversion and the time of the solid reduction period without carbon deposition increased significantly when the reaction temperature increased. It was found that carbon deposited on the carrier increased with increasing the solid reduction time. An increase in the H_2O/CH_4 molar ratio produced an increase in the time of the solid reduction period without carbon deposition, while the maximum conversion of the oxygen carriers was almost not affected. The support used and the preparation method of the carriers also influenced the reactivity and the carbon deposition.

Up to date, no studies about CLR of higher hydrocarbons than CH_4 can be found in literature. In this paper, the reaction of different oxygen carriers with a model compound representative of high temperature biomass tar is studied. This way, we evaluate the performance of these carriers in the tar-cleaning of a biomass gasification gas, focusing on the analysis of the conditions to avoid or minimize carbon deposition.

2 Experimental

2.1 Biomass tar model compound

Because of the complex composition of real tar, several researchers have studied tar decomposition reactions using biomass tar model compounds such as: anthracene [25], benzene [25–31], cyclohexane [32], 1-methyl-naphthalene [26, 33], naphthalene [25, 27, 28, 34–45], n-heptane [26, 46–48], phenol [49], pyrene [25] and toluene [10, 11, 25–28, 31, 50–57].

The selection of the right tar model for a specific process should consider the process conditions under which the tar was produced, because they determine the final tar composition. In this study, toluene has been chosen as representative of the tar formed during woody biomass gasification at high temperatures. In similar conditions, Simell et al. [51] supported the selection of toluene as tar model compound in their tar decomposition studies on dolomites and limestones, because of its relatively high stability, its presence in the tar and its well-known high-temperature chemistry [58]. Their reforming experiments indicate that quite a realistic picture of the tar-decomposition activity of the catalyst could be achieved with toluene. Toluene was fed into the reaction system by saturating a nitrogen flow at the corresponding temperature. Nitrogen bubbled through a toluene flask filled with high-purity liquid toluene (99.8%) supplied by Sigma-Aldrich. The toluene flask was placed in a water-glycol bath so that toluene temperature could be controlled. The final toluene concentration in the gas stream was set considering as a limit the values reported in literature for a high tar content in the biomass gas (ca. 7000 ppmv) [10].

2.2 Oxygen carriers

Four different carriers were tested as potential materials for CLR of biomas tar: two Ni-based samples, one Mn-based and the natural Fe-based ore, ilmenite. To make sure that ilmenite was in its most oxidized state it was first oxidized for 24 h at 1223 K in a 1 dm^3/min (STP) air stream [59]. Table 1 summarizes the composition, preparation method and some of the properties of these carriers. The oxygen capacity (R_0) is defined as:

$$R_0 = \frac{m_{ox} - m_{red}}{m_{ox}} \tag{4}$$

where m_{ox} and m_{red} are the mass of the sample when it is fully oxidized or reduced, respectively.

In the following and for a better clarity, the reference name for each of them will be used throughout this paper.

As mentioned before, many of the CLR studies until now are related to methane reforming. This is also the case of some of the carriers in Table 1. The Ni-based oxygen carriers (Ni60 and Ni40) were compared by Johansson et al. [60] in the reforming of methane at 950 °C. Ni60 had a better methane conversion. However, neither of the particles managed to avoid carbon formation at the CLR conditions tested. Nevertheless, they were considered in this study due to their high selectivity to CO and H_2. Besides, their CLR behaviour was tested in a lower temperature range (873-1073 K), as for the rest of the samples.

2.3 Experimental setups

2.3.1 Thermogravimetric analysis device (TGA)

The reactivity of the oxygen carriers was investigated in a thermogravimetric apparatus Netzsch STA 409 C operating at atmospheric pressure. The temperature range intended to be investigated was 873-1073 K, but in order to avoid toluene thermal cracking in the gas phase prior to reaction with the sample, it was limited to 873-973 K. At temperatures higher than 973 K and without the presence of water, the C_7H_8 decomposition in the gas phase took place due, mainly, to the high residence time of the reacting gas in the TGA reaction chamber. This phenomenon leads to the formation of pyrolytic carbon and soot [61].

In all the experiments, 10 mg of oxygen carrier particles sieved to a size of 180-212 μm were spread out on the bottom of an alumina crucible. The particles were well-spread in the crucible forming a single layer, in order to avoid the interparticle mass transfer resistance. The gas flow to the reactor chamber, 150 ml/min (STP), was controlled by electronic mass flow regulators. A portion of the total gas flow, i.e. 100 ml/min (STP) purge N_2, was always introduced to the bottom of the TGA to maintain the inert atmosphere in the balance chamber.

Each sample was subjected to reaction at different temperatures consecutively (873-973-873 K). At each temperature, the sample was exposed in a cyclic manner to a reducing atmosphere and to a mixture of O_2 and N_2. For Ni60, Ni40 and Mn40, the duration of the cycles were 9 minutes for reduction and 8 min for oxidation and in the case of the Fe sample, it was 30 and 25 min,

respectively. Eight reducing-oxidizing cycles were carried out. Nitrogen was introduced between reducing and oxidizing steps during 3 minutes to avoid mixing gaseous atmospheres. During the reducing period, the sample was exposed to a C_7H_8 + H_2O stream. As toluene gas solubility in water is low, this stream was obtained by first saturating a 50 ml/min (STP) N_2 flow at 270.5 K with C_7H_8 and after with H_2O at 333 K. Concentrations of both reactants in the gas phase resulted in 0.25% and 6.67%, respectively, which correspond to a H_2O/C_7H_8 molar ratio of 26.4. During the solid oxidizing period, the particles were regenerated in the presence of 6.67% O_2 in N_2.

2.3.2 Fixed bed flow reactor (FB)

The FB experiments were conducted in a quartz fixed bed reactor of 17 mm internal diameter and 610 mm length. The solid sample (150-400 mg) was placed on a thin quartz wool bed on a porous plate in the middle of the reactor. The porous plate had a pore size of 90-150 μm. Solid samples were sieved and the size range 212-250 μm was used in the experiments as a compromise between mass transfer limitations and problems of feeding very fine particles into the system. The reactor was located inside an electrically heated oven, with three independent zones for controlling the temperature. The temperature profiles in the reactor were measured at non-reacting conditions (2 dm^3/min N_2 (STP)) with a K thermocouple in the proximities of the porous plate where the reaction took place. The uncertainty of the thermocouple measurement was $\pm$ 1.5 K. The four oxygen carriers were tested in the temperature range 873-1073 K. The residence time of the reactant gases in the reaction zone was much lower than in the TGA and this prevented toluene from thermal cracking. A manometer connected to the inlet line measured the reactor pressure. A con-

trol panel connected to mass flow controllers was used to prepare the mixture of gases to be fed to the reactor. Toluene was fed by saturating a N_2 stream at 288 K. The water was fed to the system by saturating a N_2 flow with H_2O at 313 K in an evaporator. The total reactant gas flow to the reactor was maintained at 2.0 dm^3/min (STP) and the reactor pressure was around 0.11 MPa.

The product gas was cooled in a condenser and the water removed. The composition of the dry product gas from the reactor was analyzed through a continuous gas analyzer. A Rosemount NGA 2000 MLT infrared gas analyzer determined the concentration of O_2, CO, and CO_2. The accuracy in the measured concentration was below or equal to 1% of the measurement range, and the typical measurement ranges were set to be 0-2% for O_2 and 0-5000 or 0-2% for CO and CO_2. The sensitivity of this analyzer was estimated as less or equal to 1% of the range used. All data from each experiment (temperature, pressure and concentrations as a function of time) were logged in a file.

The reactor was heated to the desired temperature and then the gaseous mixture was fed. The samples experienced consecutive reducing and oxidizing cycles. Seven cycles were performed with each sample except in the case of ilmenite. Previous studies with iron oxide particles have shown differences in reactivity during the first cycles before stabilizing [62]. Therefore, in this case the number of cycles was thirteen. A nitrogen flow cleaned the reactor during 2 minutes between the reducing and subsequent oxidizing step. After each experiment, the sample was taken out of the reactor by removing the bottom part of it.

Table 2 presents the gaseous systems and parameters that have been analyzed: temperature, time for the solid reduction step (t_R) and H_2O/C_7H_8 molar ratio.

3 Results and discussion

3.1 Thermogravimetrical analysis

The TGA experiments were designed to analyze the carbon deposition on the samples so that the different steps in the reaction of the carriers were observed. Figure 2 shows these steps. First, the sample reacts in the presence of C_7H_8 and H_2O (reducing step). Initially, the transfer of oxygen takes place and the sample weight decreases up to a point at which this transfer is overcome by carbon deposition. The carbon deposit makes the weight of the sample increase again. Following the reducing step, a nitrogen flow is introduced so that the remaining gases from the reducing step are removed. Then, the oxidizing mixture is introduced. During the initial moments, the deposited carbon is burned off in the presence of oxygen, which results in a decrease of the sample weight. After this, the regeneration of the carrier to the initial weight of the sample introduced occurs.

In the present TGA configuration, the reacting gases diffuse down the crucible until they reach the oxygen carrier sample at the bottom of it. The diffusion rate to the bottom was estimated and compared to some of the observed reaction rates, to check the possible diffusion limitations that may exist in this specific experimental configuration but none were encountered, i. e. the maximum mass transfer rate was higher than the observed reaction rates.

When Ni40 reacts with C_7H_8 and H_2O, the weight loss in the reduction step increases with the number of cycles for all the temperatures tested. Figure 3 shows this for the 1^{st}, 4^{th} and 8^{th} cycle at 873 K (both sets) and 973 K. The maximum weight loss observed in the reaction of Ni40 with C_7H_8 and H_2O

(at 973 K) was around 44% of the oxygen capacity, R_0 (0.086). However, no final carbon deposit is observed in any case. Besides, in the reduction step there seems to be two different stages. First, a fast oxygen transfer from the carrier followed by a slower weight loss rate. Similar curves have been observed before in CLC applications when working with NiO carriers supported on $NiAl_2O_4$ [63]. In those cases, the first stage was correlated to the fast reduction of the free NiO phase and the second one to the slow reduction of $NiAl_2O_4$. It is also interesting to note that the Ni40 oxidation rate becomes a bit slower with the number of cycles, pointing to the possibility of some kind of deactivation of the carrier.

The weight loss of Mn40 sample in the reduction step is almost constant from the first cycle for all the temperatures tested as Figure 4 shows. At the lowest temperature (873 K), it can be considered stable from the fourth cycle. But at 973 K is the same for all the cycles showed in the graph. It is also interesting to note that Mn40 exhibits a high reactivity with no carbon deposition at any temperature. The weight loss is close to the maximum value given by R_0 (0.028) at both 873 and 973 K. Similar oxidation rates were observed at each temperature for the different cycles.

Fe also shows an increase in the weight loss in the reduction step with the number of cycles at 973 K (not shown). In this case, some reactivity was observed in the second step at 873 K. The maximum weight loss of the sample is still low compared to R_0 (no more than 20%) but again, no carbon deposition was observed.

As mentioned before, each sample reacted consecutively at 873-973-873 K with approximately 0.25% C_7H_8 in a H_2O/C_7H_8 molar ratio of 26.4. This experimental approach allowed detecting in some of the carriers an increase

in the maximum weight loss registered in the reduction period in the second set of cycles at 873 K, after reacting at 973 K. Figure 5 shows this behaviour for the 8^{th} cycle in the experiments with Ni40 (top) and Mn40 (bottom). The maximum weight loss for Ni40 in the second set at 873 K is higher (down to 96.25%) when compared to the first set (down to 98.5%). Besides, the oxidation in the second set seems to be slower. For Mn40, the change in the maximum weight loss was much less and the oxidation rate was similar in both sets. Finally, although not shown, this effect was also observed in the Fe carrier, which showed some reactivity in the second set at 873 K while it did not show any in the first one. Nevertheless, the maximum weight loss for this carrier was very small.

The Ni60 sample showed no reactivity at any of the temperatures tested. Some sample was collected after reaction with C_7H_8 and H_2O and further analyzed. The reacted sample was observed with a Scanning Electron Microscope and no relevant changes in morphology were found. XRD analysis allowed to investigate the species present in the sample after reaction and compare them with the ones present in the original sample. This analysis did not reveal any change either. This subject might be further investigated, but according to the present indications, Ni60 cannot be considered as a promising material for biomass tar reforming.

For a better comparison of the reactivity of the different carriers the mass-based conversion (ω) was considered. This parameter is defined as:

$$\omega = \frac{m}{m_{ox}} \tag{5}$$

where m is the actual mass of the sample and m_{ox} is the mass of the sample

when it is fully oxidized. The mass-based rate can be then calculated as $d\omega/dt$.

Figure 6 shows the rate of mass conversion, $d\omega/dt$, as a function of mass conversion (ω) for the 8^{th} reduction step at the highest temperature tested (973 K) for experiments with C_7H_8 and H_2O and the four oxygen carriers. The mass rate is maximum at the beginning of the experiment, when there is plenty of oxygen to be transferred, and decreases while mass conversion decreases. The decrease in the mass rate is faster in the experiment with Ni40 compared to that of Mn40. Nevertheless both present a similar value of final mass conversion. This could be attributed to a competition between simultaneous processes taking place in the case of Ni40, i. e. carrier consumption, carrier regeneration by water and carbon deposition and subsequent gasification. Previous studies [64, 65] have proposed that carbon formation followed by:

$$C(s) + H_2O \longrightarrow CO + H_2 \tag{6}$$

may be a possible reaction path for NiO on $NiAl_2O_4$ particles. Thus, one can not exclude the possibility that carbon could be an intermediate also when no carbonaceous species are leaving the reactor in the oxidizing period. It might be that carbon formation occurs but at a rate where it is rapidly gasified. Finally, it is visible again that Fe shows a very low rate.

In summary, no final carbon deposition was observed in the TGA experiments in the temperature range 873-973 K when working with a H_2O/C_7H_8 molar ratio of 26.4. However, Ni60 showed no reactivity in the conditions analyzed and Fe reactivity was very low at the temperatures tested.

3.2 Fixed bed flow reactor

In the fixed bed reactor, experiments with Ni40, Mn40 and Fe were performed. Considering the previous results where Ni60 showed no reactivity, this carrier was not further tested. As mentioned before, the experiments in the fixed bed reactor allowed investigating higher temperatures (1073 K) and also the reactivity of the carriers towards C_7H_8 without the presence of water. The concentrations of CO, CO_2 and O_2 were measured for the reduction and oxidation step of each cycle. Those measurements were used to extract information about carbon deposition during the process, which is the main objective of this work.

The moles of carbon deposited were calculated from the CO and CO_2 concentrations during the oxidizing step:

$$C_{deposited} = F_{oxi} \cdot \int_{t_0}^{t_{oxi}} (C_{CO_{oxi}} + C_{CO_{2,oxi}}) dt \tag{7}$$

where $C_{CO_{oxi}}$ and $C_{CO_{2,oxi}}$ are CO and CO_2 concentrations in the outlet stream and F_{oxi} is the molar flow in the oxidizing period.

In a similar way, the moles of carbon released as CO and CO_2 in the reducing period were calculated:

$$C_{reducing} = F_{red} \cdot \int_{t_0}^{t_{red}} (C_{CO_{red}} + C_{CO_{2,red}}) dt \tag{8}$$

where $C_{CO_{red}}$ and $C_{CO_{2,red}}$ are CO and CO_2 concentrations in the outlet stream and F_{red} is the molar flow in the reducing period.

Finally, the moles of oxygen that were transferred by the carrier during the reducing period were estimated as:

$$O_{reacted} = F_{oxi} \cdot \int_{t_0}^{t_{oxi}} (2 \cdot (C_{O_{2,0}} - C_{O_2}) - (C_{CO_{oxi}} + 2 \cdot C_{CO_{2,oxi}}))dt \qquad (9)$$

where $C_{O_{2,0}}$ is the initial oxygen concentration in the gas stream and C_{O_2} the oxygen concentration at different times.

These values were used in the calculation of the following parameters:

- Percentage of carbon deposited in the reducing step (C_{dep})

$$C_{dep} = \frac{C_{deposited}}{C_{introduced}} \cdot 100 \qquad (10)$$

- Solid conversion in the reducing step (X_O)

$$X_O = \frac{O_{reacted}}{O_{introduced}} \qquad (11)$$

- Carbon conversion in the reducing step (X_c)

$$X_c = \frac{C_{deposited} + C_{reducing}}{C_{introduced}} \qquad (12)$$

In this case it is assumed that the only carbonaceous products in the reaction of the carrier with toluene (without or with water) are CO and CO_2.

In the following, the effect on these parameters of different operating conditions will be addressed.

3.2.1 Effect of temperature

Figure 7 compares the evolution of the carbon deposition percentage and the solid conversion with the number of cycles in the experiments of Ni40 with only C_7H_8.

At 1073 K, the amount of carbon deposited is more or less stable from the fourth cycle (around 30%), as it is the solid conversion, which is close to 0.9. At 873 K, both carbon deposited and solid conversion increase with the number of cycles, with a maximum value of approximately 7.5% and 0.45, respectively. It is interesting to see the tendency of Ni40 to carbon deposition, specially at the highest temperature. When no water is present, temperature is therefore a key parameter to control carbon deposition.

Figure 8 presents the effect of temperature on the reaction of Mn40 with C_7H_8 in similar conditions. In this case, the amount of carbon deposited at both 1073 K and 873 K was similar for all the cycles from the beginning. It was only a small amount (2.5% at the most), specially at the lowest temperature. This suggest that the main path for carbon deposition would be toluene decomposition through reaction (3):

$$C_7H_8 \rightleftharpoons 7\,C(s) + 4\,H_2 \tag{3}$$

and not the Bouduard reaction (reaction (1)) or reaction (2). Besides, the solid conversion was complete at both temperatures.

Results for the Fe carrier reaction with C_7H_8 at 1073 K and 873 K are shown in Figure 9. This carrier needed more initial cycles than the others to show some reactivity, which, as it is shown, increases with the number of cycles. At

1073 K, the maximum percentage of carbon deposited (4.5%) was higher than in the case of Mn40 and the maximum solid conversion was low compared to both Ni40 and Mn40, as it was also observed in the TGA experiments. At 873 K, almost no reactivity and little carbon formation was observed. Corbella and Palacios [66] also noted that the reactivity of different iron oxide carriers is comparatively lower than that exhibited by CuO and NiO based carriers tested at similar conditions.

Leion et al. [67] concluded that the oxidation/reduction of the ilmenite proceeded between the reduced form ilmenite $FeTiO_3$ and the oxidized form $FeTiO_5$ + TiO_2, with the likely intermediate Fe_2O_3 or $Fe_2O_3{\cdot}TiO_2$, although other intermediates could not be completely excluded. In Figure 9, the point at which carbon deposition starts to increase significantly seems to be correlated with the initiation of the solid conversion. According to this result, it could be speculated that the carbon deposition might be catalized by $FeTiO_3$.

3.2.2 Effect of the time for the reduction step

The FB experiments allowed testing the influence of the time for the reducing step on the amount of carbon deposited and solid conversion in experiments with C_7H_8 and no H_2O. Ni40, Mn40 and Fe were tested under three different reduction times (4, 3, and 1.5 minutes) at different temperatures. Figure 10 shows the results for Ni40. At 1073 K (Figure A) it can be observed that the carbon deposited and the solid conversion are more or less stable from the fourth cycle. The amount of carbon deposited is decreased up to 2 times when the reduction time for the reducing step decreases from 4 to 1.5 minutes. The values of solid conversion also decrease to a value around 0.5. At 873 K (Figure B), the effect of the reduction time on the amount of carbon deposited

is not that clear. No big differences were observed in the percentages for the three times tested. Figure 10 C shows the values of carbon conversion for the different reduction times at the two temperatures. At 1073 K, the carbon conversion in the last cycles varies between 0.6 and 0.4 for 4 and 3-1.5 minutes, respectively. At 873 K, the values drop to around 0.15-0.2 for all the reducing times used.

Figure 11 presents the effect on carbon deposition and solid conversion when different reaction times (4, 3, and 1.5) are used in the reaction of Mn40 with C_7H_8 at 1073 K (Figure A) and 873 K (Figure B). No significant differences were observed at any of the temperatures, which could be an indication of the carbon deposition taking place during the time when there is still oxygen left in the carrier and not when it has been completely reduced. At 1073 K, Figure 11 C shows carbon conversions around 0.15 for the different reduction times tested. At 873 K, the values were around 0.05.

Figure 12 shows how at 1073 K (Figure A) a decrease in the reduction time from 4 to 1.5 minutes decreases significantly the amount of carbon deposited on the Fe carrier (from a maximum of 4.5% to around 1%). Figure B presents the values of the calculated carbon conversion, which rise up to 0.075.

3.2.3 Effect of water presence

As shown in Table 1, high values of H_2O/C_7H_8 were tested, according to the findings of Adánez et al. for light hydrocarbons [68]. They performed thermodynamic calculations to evaluate the possibility of carbon formation regarding the use of light hydrocarbons as fuel in a CLC process in the presence of a Ni-based oxygen carrier supported on alumina. The H_2O to fuel ratio needed

to avoid carbon formation was higher the higher the hydrocarbon and the lower the temperature, which shows the higher tendency to carbon formation of higher hydrocarbons compared to pure CH_4. As a general rule, they found that the H_2O/HC ratio to avoid carbon formation tends to n as temperature increases, where n is the number of carbon atoms in the hydrocarbon (HC).

The effect of the addition of water on the Ni40-C_7H_8 reaction was analyzed for different H_2O/C_7H_8 molar ratios (4.5 and 8) both at 873 and 1073 K. This way the information obtained from the TGA experiments was completed with results at higher temperatures and lower H_2O/C_7H_8 molar ratios. Figure 13 shows the results for both temperatures. At 1073 (Figure A) it was observed that the carbon deposited decreased up to 6 times for the highest H_2O/C_7H_8 molar ratio. It is possible that a further increase in the H_2O/C_7H_8 ratio would lead to a further carbon deposition reduction if one considers the results from the TGA experiments, where a H_2O/C_7H_8 ratio of 26.4 was used at a lower temperature (973 K) and no carbon deposition was observed. At this high temperature, the solid conversion decreased from 0.87 down to around 0.75. This might be the result of the competition between the reduction of the carrier and its reoxidation by water. At 873 K (Figure B) a decrease in the amount of carbon deposited was also observed when increasing the H_2O introduced, although this time the reduction was around 2 times the initial value. Finally, Figure 13 C does not show significant changes in the final values of carbon conversion at 1073 K (around 0.5) and 873 K (around 0.18).

Figure 14 presents the effect of water addition in the Mn40-C_7H_8 reaction at both 1073 K (Figure A) and 873 K (Figure B). At 1073 K, the addition of water in H_2O/C_7H_8 ratios of 16.9 and 33.6 causes in both cases a reduction of the amount of carbon deposited. At 873 K, the addition of H_2O in a H_2O/C_7H_8

ratio of 16.9 decreases the amount of carbon deposited to almost negligible, although that was accompanied by an important decrease in the solid conversion. Figure 14 C shows an increase in the values of carbon conversion (0.1 to 0.2) when water was introduced at 1073 K.

Figure 15 presents the effect of water addition in the Fe-C_7H_8 reaction at 1073 K (Figure A). The presence of H_2O decreases the maximum amount of carbon deposited from 4.5 to 0.5%, although no big differences in the final carbon deposited were observed for the two H_2O/C_7H_8 molar ratios tested (10.1 and 20.2). Besides, the solid conversion when water was added dropped to almost zero, indicating that the solid is kept in the oxidized form. Figure 15 C shows no significant changes in the final carbon conversion values at 1073 K.

4 Practical implications

The experimental results presented in this work point to Ni40 and Mn40 as the most promising carriers to be used in CLR of biomass tar. Both showed reactivity to C_7H_8 in the temperature range studied (873-1073 K) and stabilized quickly after a few cycles when reacting, even from the beginning in the case of Mn40. Ni40 showed a change in the reactivity after reaction at high temperatures, which is interesting for the practical aspects in the operation with this carrier. It is possible to increase its reactivity at such low temperatures as 873 K by previously activating the carrier in the same atmosphere but at higher temperatures.

Ni40 shows more tendency to form carbon than Mn40 when reacting with C_7H_8. The carbon amount deposited is influenced by the process temperature. The deposited carbon notably increases with temperature, specially

when working with Ni40. In this case the control of the temperature in the fuel reactor, and therefore the solid circulation rate in the CL system, is critical for an operation without carbon losses due to carbon deposition. The reduction of the reaction time between Ni40 and C_7H_8 decreases the carbon deposition and the global carbon conversion is also lowered, affecting the removal of C_7H_8. The addition of H_2O is effective in decreasing the amount of carbon deposited, but high H_2O/C_7H_8 ratios are required compared to those used in the reforming of other hydrocarbons, such as CH_4. This also affects the energy balance in the system and therefore, the solid circulation rate, which has to be adjusted to allow the endothermic reactions in the fuel reactor to take place. In this study, carbon formation on Ni40 and Mn40 was avoided with a H_2O/C_7H_8 molar ratio of 26.4.

5 Concluding remarks

An experimental study to evaluate the suitability of different oxygen carriers in chemical looping reforming of biomass tar has been carried out with toluene as tar model compound. The conditions in which carbon deposition is minimized have been investigated. The main conclusions that can be extracted from the study are:

- Ni60 showed no reactivity to C_7H_8 and H_2O in the TGA experiments. The activation of the carrier after previous reaction at higher temperatures was observed in the case of Ni40, Mn40 and Fe.
- Ni40 behaviour became quickly stable with the number of cycles at 1073 K. Mn40 reactivity was stable almost from the first cycle in the 873-1073 K temperature range. Besides, the oxygen transfer observed in Mn40 experi-

ments was close to the maximum represented by R_0. Fe reactivity showed an increase with the number of cycles at the different temperatures tested in all the experiments. Ni40 and Mn40 showed similar values of final mass conversion when reacting with a H_2O/C_7H_8 molar ratio of 26.4 at 973 K in the TGA. In the same conditions, Fe mass rates were very low.

- Regarding carbon deposition, Ni40 showed a high tendency to carbon formation when reacting with only C_7H_8, specially at 1073 K. In this case, the carbon deposited could be decreased by decreasing the temperature, the time assigned for the reduction step and increasing the H_2O/C_7H_8 molar ratio. Mn40 showed low tendency to form carbon when reacting with C_7H_8 both at 1073 and 873 K. The amount of carbon deposited was not affected by the decrease in the reduction time. Water addition reduced the amount of carbon formed at 1073 K. Fe showed a low reactivity to C_7H_8 after some cycles at 1073 K. At 873 K, no reactivity was observed.

6 Acknowledgments

This project is part of the Era-Net Bioenergy project *Energy efficient selective reforming of hydrocarbons*. The authors thank the funding received from Energinet.dk.

References

[1] Devi L, Ptasinski KJ, Janssen FJJG. A review of the primary measures for tar elimination in biomass gasification processes. Biomass Bioenergy 2003;24:125-40.

[2] Kirubakaran V, Sivaramakrishnan V, Nalini R, Sekar T, Premalatha M, Subramanian P. A review of gasification of biomass. Renewable Sustainable Energy Rev 2009; 13: 179-86.

[3] Milne TA, Evans RJ, Abatzoglou N. Biomass gasifier "tars": their nature, formation and conversion, NREL Report NREL/TP-570-25357, Colorado, 1998.

[4] Evans RJ, Knight RA, Onischak M, Babu SP. Development of biomass gasification to produce substitute fuels, Richland, WA: Pacific Northwest Laboratory, PNL-6518, 1988.

[5] Corella J. Thermochemical Biomass Conversion: Upgrading of the Crude Gasification Product Gas, Final Synthesis Report, Agro-Industrial Research, EC/AIR, project: AIR2-CT93-1493, 1996.

[6] Dayton DC, Evans RJ. Laboratory gasification studies via partial oxidation of biomass pyrolysis vapors. In: Overend R P, Chornet E, editors. Proceedings of the 3^{rd} Biomass Conference of the Americas Vol.1., Canada; 1997, p. 673-82.

[7] Orío A, Corella J, Narváez I. Performance of different dolomites on hot raw gas cleaning from biomass gasification with air. Ind Eng Chem Res 1997;36:3800-8.

[8] Dayton D. A review of the literature on catalytic biomass tar destruction, NREL project: NREL/TP-510-32815, 2002.

[9] Trimm DLA. Catalysts for the control of cocking during steam reforming. Catal Today 1999;49:3-10.

[10] Świerczyński D, Courson C, Kiennemann A. Study of steam reforming of toluene used as model compound of tar produced by biomass gasification. Chem Eng Process 2008;47:508-13.

[11] Simell PA, Kurkela EA. Effects of gasification gas components on tar and ammonia decomposition over hot gas cleanup catalysts. Fuel 1997;76:1117-27.

[12] Rostrup-Nielsen JR. In: Anderson J R, Boudart M, editors. Catalysis Vol.5., Springer-Verlag, Berlin, 1984, p. 75.

[13] Richter H, Knoche K. Reversibility of combustion processes. ACS Symposium Series 1983;235:71-86.

[14] Ishida M, Zheng D, Akehata T. Evaluation of chemical-looping-combustion power-generation system by graphic exergy analysis. Energy 1987;12:147-54.

[15] Lyngfelt A, Leckner B, Mattisson T. A fluidized-bed combustion process with inherent CO_2 separation: application of chemical-looping combustion. Chem Eng Sci 2001;56:3101-13.

[16] Adánez J, de Diego LF, García-Labiano F, Gayán P, Abad A, Palacios JM. Selection of oxygen carriers for chemical looping combustion. Energy Fuels 2004;85:371-7.

[17] Cho P, Mattisson T, Lyngfelt A. Comparison of iron-, nickel-, copper- and manganese-based oxygen carriers for chemical-looping combustion. Fuel 2004;83:1215-25.

[18] Rydén M, Lyngfelt A, Mattisson T, Chen D, Holmen A, Bjørgum E. Novel oxygen carrier materials for chemical-looping combustion and chemical-looping reforming; $La_xSr_{1-x}Fe_yCo_{1-y}O_{3-\delta}$. Int J Greenh Gas Con 2008;2:21-36.

[19] Zafar Q, Mattisson T, Gevert B. Integrated hydrogen and power production with CO_2 capture using chemical-looping reforming–Redox reactivity of particles of CuO, Mn_2O_3, NiO and Fe_2O_3 using SiO_2 as support. Ind Eng Chem Res 2005;44:3485-96.

[20] Zafar Q, Mattisson T, Gevert B. Redox investigation of some oxides of transition-state metals Ni, Cu, Fe and Mn supported on SiO_2 and $MgAl_2O_4$. Energy Fuels 2006;20:34-44.

[21] Rydén M, Johansson M, Lyngfelt A, Mattisson T. NiO supported on Mg-ZrO_2 as oxygen carrier for chemical-looping combustion and chemical-looping reforming. Energy Environ Sci 2009;2:970-81.

[22] Rydén M, Lyngfelt A, Mattisson T. Synthesis gas generation by chemical-looping reforming in a continuously operating laboratory reactor. Fuel 2006;85:1631-41.

[23] Rydén M, Lyngfelt A, Mattisson T. Chemical-looping combustion and chemical-looping reforming in a circulating fluidized-bed reactor using Ni-based oxygen carriers. Energy Fuels 2008;22:2585-97.

[24] de Diego LF, Ortiz M, Adánez J, García-Labiano F, Abad A, Gayán P. Synthesis gas generation by chemical-looping reforming in a batch fluidized bed reactor using Ni-based oxygen carrier. Chem Eng J 2008;144:289-98.

[25] Coll R, Salvadó J, Farriol X, Montané D. Steam reforming model compounds of biomass gasification tars: conversion at different operating conditions and tendency towards coke formation. Fuel Process Technol 2001;74:19-31.

[26] Ellig DL, Lai CK, Mead DW, Longwell JP, Peters WA. Pyrolysis of volatile aromatic hydrocarbons and n-heptane over calcium oxide and quartz. Ind Eng Chem Process Des Dev 1985;24:1080-87.

[27] Jacoby WA, Gebhard SC, Vojdani RL. Lifetime testing of catalysts for biosyngas conditioning-single versus dual catalysts comparison, Thermochemical conversion-process research branch C-Milestone completion report, 1995.

[28] Jess A. Mechanisms and kinetics of thermal reactions of aromatic hydrocarbons from pyrolysis of solid fuels. Fuel 1996;75:1441-48.

[29] Simell PA, Hakala NAK, Haario HE. Catalytic decomposition of gasification gas tar with benzene as the model compound. Ind Eng Chem Res 1997;36:42-51.

[30] Simell PA, Hirvensalo EK, Smolander VT, Krause AOI, Steam reforming of gasification gas tar over dolomite with benzene as a model compound. Ind Eng Chem Res 1999;38:1250-57.

[31] Zhang R, Wang Y, Brown RC. Steam reforming of tar compounds over Ni/olivine catalysts doped with CeO_2. Energy Convers Manage 2007;48:68-77.

[32] Taralas G. Cyclohexane-steam cracking catalysed by calcined dolomite $CaMgO_2$. In: Bridgwater A V, Boocock DGB, editors. Developments in thermochemical biomass conversion, Vol.2., Blackie Academic & Professional, London, 1997, p. 1086-1100.

[33] Dou B, Gao J, Sha X, Baek SW. Catalytic cracking of tar component from high-temperature fuel gas. Appl Therm Eng 2003;23:2229-39.

[34] García XA, Hüttinger KJ. Steam gasification of naphthalene-catalyst-calcium oxide. Erdoel, Kohle, Erdgas, Petrochem 1990;43:273-81.

[35] Aldén H, Bjrkman E, Carlsson M, Waldheim L. Catalytic cracking of naphthalene on dolomite. In: Bridgwater A V, editor. Advances in Thermochemical Biomass Conversion Vol.1., Blackie Academic & Professional, London, 1993, p. 216-32.

[36] Espenäs BG. The kinetics of conversion of naphthalene into H_2 and CO catalysed by dolomite. In: Chartier P, editor. 9^{th} European Bioenergy Conference & 1^{st} European Energy from Biomass Technology Exhibition, Pergamon, Copenhagen, 1996, pp. 270.

[37] Lammers G, Orío A, Beenackers AACM. Catalytic tar removal from biomass producer gas with in-situ catalyst regeneration. In: Chartier P, editor. 9^{th} European Bioenergy Conference & 1^{st} European Energy from Biomass Technology Exhibition, Pergamon, Copenhagen, 1996, p. 1416-22.

[38] Bangala DN, Abatzoglou N, Martin JP, Chornet E. Catalytic gas conditioning-

Application to biomass and waste gasification. Ind Eng Chem Res 1997;36:4184-92.

[39] Lammers G, Beenackers AACM, Corella J. Catalytic tar removal from biomass producer gas with secondary air. In: Bridgwater A V, Boocock DGB, editors. Developments in thermochemical biomass conversion, Vol.2., Blackie Academic & Professional, London, 1997, p. 1179-93.

[40] Bangala DN, Abatzoglou N, Chornet E. Steam reforming of naphthalene on Ni-Cr/Al_2O_3 catalyst doped with MgO, TiO_2 and La_2O_3. AIChE J 1998;44:927-36.

[41] Devi L, Ptasinski KJ, Janssen FJJG. Pretreated olivine as tar removal catalyst for biomass gasifiers: investigation using naphthalene as model biomass tar. Fuel Process Technol 2005;86:707-30.

[42] Furusawa T, Tsutsumi A. Development of cobalt catalysts for the steam reforming of naphthalene as a model compound of tar derived from biomass gasification. Appl Catal A 2005;278:195-205.

[43] Furusawa T, Tsutsumi A. Comparison of Co/MgO and Ni/MgO catalysts for the steam reforming of naphthalene as a model compound of tar derived from biomass gasification. Appl Catal A 2005;278:207-12.

[44] Houben MP, de Lange HC, van Steenhoven AA. Tar reduction through partial combustion of fuel gas. Fuel 2005;84:817-24.

[45] Wang CG, Wang TJ, Ma LL, Gao Y, Wu CZ. Partial oxidation reforming of biomass fuel gas over nickel-based monolithic catalyst with naphthalene as model compound. Korean J Chem Eng 2008;25:738-43.

[46] Taralas G, Vassilatos V, Sjöström K, Delgado J. Thermal and catalytic cracking of n-heptane in presence of calcium oxide, magnesium oxide and calcined dolomites. Can J Chem Eng 1991;69:1413-19.

[47] Taralas G, Sjöström K, Bjornbom E. Dolomite catalyzed cracking of n-heptane in presence of steam. In: Bridgwater AV, editor. Advanced thermochemical biomass conversion, Vol.3., Blackie Academic & Professional, London, 1994, p. 233-45.

[48] Taralas G. Catalytic steam cracking of n-heptane with special reference to the effect of calcined dolomite. Ind Eng Chem Res 1996;35:2121-26.

[49] Pedersen K. Catalytic tar cracking, Danish Technological Institute, DK-8000, Aarkas C., 1994, p. 13.

[50] Gebhard SC. Evaluation and modeling of catalysts for methanol syngas conditioning, Chemical Technologies Research Branch Milestone Completion Report, Methanol Syngas Conditioning, BF153434, 1992.

[51] Simell PA, Lepplahti JK, Kurkela EA. Tar/decomposing activity of carbonate rocks under high CO_2 partial pressure. Fuel 1995;74:938-45.

[52] Taralas G, Kontominas MG, Katatsios X. Modeling the thermal destruction of toluene (C_7H_8) as tar-related species for fuel gas cleanup. Energy Fuels 2003;17:329-37.

[53] Juutilainen SJ, Simell PA, Krause AOI. Zirconia: Selective oxidation catalyst for removal of tar and ammonia from biomass gasification gas. App Catal B-Environ 2006;62:86-92.

[54] Bona S, Guillén P, Alcalde GJ, García L, Bilbao R. Toluene steam reforming using coprecipitated Ni/Al catalysts modified with lanthanum or cobalt. Chem Eng J 2008;137:587-97.

[55] Pansare SS, Goodwin JG Jr, Gangwal S. Toluene decomposition in the presence of hydrogen on tungsten-based catalysts. Ind Eng Chem Res 2008;47:4077-85.

[56] Świerczyński D, Libs S, Courson C, Kiennemann A. Steam reforming of tar from biomass gasification process over Ni/olivine catalyst using toluene as a

model compound. App Catal, B-Environ 2007;74:211-22.

[57] Lamacz A, Krztoń A, Musi A, Da Costa P. Reforming of model gasification tar compounds. Catal Lett 2009;128:40-8.

[58] Poutsma ML. Free-Radical Thermolysis and hydrogenolysis of model hydrocarbons relevant to processing of coal. Energy Fuels 1990;4:113-31.

[59] Leion H, Mattisson T, Lyngfelt A. Solid fuels in chemical-looping combustion. Int J Greenhouse Gas Control 2008;2:180-93.

[60] Johansson M, Mattisson T, Lyngfelt A, Abad A. Using continuous and pulse experiments to compare two promising nickel-based oxygen carriers for use in chemical-looping technologies. Fuel 2008;87:988-1001.

[61] Bruinsma OSL, Geertsma RS, Bank P, Moulijn JA, Gas phase pyrolysis of coal-related aromatic compunds in a coiled tube flow reactor. Fuel 1988;67:327-33.

[62] Mattisson T, Johansson M, Lyngfelt A. Multicycle reduction and oxidation of different types of iron oxide particles - Application for chemical-looping combustion. Energy Fuels 2004;18:628-37.

[63] Adánez J, Dueso C, de Diego LF, García-Labiano F, Gayán P, Abad A. Methane combustion in a 500 W_{th} chemical-looping combustion system using an impregnated Ni-based oxygen carrier. Energy Fuels 2009;23:130-42.

[64] Cho P, Mattisson T, Lyngfelt A. Carbon formation on nickel and iron oxide-containing oxygen carriers for chemical-looping combustion. Ind Eng Chem Res 2005;44:668-76.

[65] Mattisson T, Johansson M, Jerndal E, Lyngfelt A. The reaction of $NiO/NiAl_2O_4$ particles with alternating methane and oxygen. Can J Chem Eng 2006;86:756-67.

[66] Corbella BM, Palacios JM. Titania-supported iron oxide as oxygen carrier for chemical-looping combustion of methane. Fuel 2007;86:11322.

[67] Leion H, Lyngfelt A, Johansson M, Jerndal E, Mattisson T. The use of ilmenite as an oxygen carrier in chemical-looping combustion. Chem Eng Res Des 2008;86:1017-26.

[68] Adánez J, Dueso C, de Diego LF, García-Labiano F, Gayán P, Abad A. Effect of fuel gas composition in chemical-looping combustion with Ni-based oxygen carriers. 2. Fate of light hydrocarbons. Ind Eng Chem Res 2009;48:2509-18.

[69] Mattisson T, Johansson M, Lyngfelt A. The use of NiO as an oxygen carrier in chemical-looping combustion. Fuel 2006;85:736-47

[70] Zafar Q, Abad A, Mattisson T, Gevert B. Reaction kinetics of freeze-granulated $NiO/MgAl_2O_4$ oxygen carrier particles for chemical-looping combustion. Energy Fuels 2007;21:610-8.

[71] Johansson M, Mattisson T, Lyngfelt A. Comparison of oxygen carriers for chemical-looping combustion. Therm Sci 2006;10:93-107.

[72] Johansson M, Mattisson T, Lyngfelt A. Use of $NiO/NiAl_2O_4$ particles in a 10kW chemical-looping combustor. Ind Eng Chem Res 2006;45:5911-9.

[73] Johansson M, Mattisson T, Lyngfelt A. Investigation of Mn_3O_4 with stabilized ZrO_2 for chemical-looping combustion. Chem Eng Res Des 2006;84:807-18.

Tables

Table 1
Main characteristics of the oxygen carriers

Reference Name	**Ni60** [69–71]	**Ni40** [71, 72]	**Mn40** [73]	**Fe** [67]
Composition	60% NiO	40% NiO	40% Mn_3O_4	94.3% $FeTiO_3$
	40% $MgAl_2O_4$	60% $NiAl_2O_4$	60% Mg-ZrO_2	
Production	FG[a]	FG[a]	FG[a]	Mineral
Calcination T / K	1673	1873	1423	-
Particle density / kg m^{-3}	3200	3800	2260	3600
Porosity	0.42	0.36	0.58	—
BET surface area / m^2 g^{-1}	1.24	0.4	—	0.11
Oxygen capacity (R_0) w/w	0.129	0.086	0.028	0.05

[a] FG: Freeze granulation

Table 2
Fixed bed experiments with the different oxygen carriers and C_7H_8

Sample	**T / K**	**[C_7H_8] / ppm**	**H_2O/C_7H_8**	**t_R / min**	**[O_2] / %**	**N_{cycles}**
Ni40	873 - 1073	2000	0	4 - 3 - 1.5	0.9	7
Mn40	873 - 1073	600	0	4 - 3 - 1.5	0.5	7
Fe	873 - 1073	1000	0	4 - 1.5	0.5	13
Ni40	873 - 1073	2000	4.5 - 8	4	0.9	7
Mn40	873 - 1073	600	17 - 33.5	4	0.5	7
Fe	873 - 1073	1000	10 - 20	4	0.5	13

Time for oxidation (t_O) in all the experiments: 6 min

List of Figure Captions

Fig. 1 Chemical Looping Reforming

Fig. 2 Expected steps in a TGA experiment with the four different carriers: percentage of weight loss (w/w_0) with time

Fig. 3 Comparison of the percentage of weight loss (w/w_0) with time for the 1^{st}, 4^{th} and 8^{th} cycle in the experiment of Ni40 with C_7H_8 (0.25%) and H_2O (6.67%). Times for reduction, purge and oxidation periods have been indicated by vertical dashed lines

Fig. 4 Comparison of the percentage of weight loss (w/w_0) with time for the 1^{st}, 4^{th} and 8^{th} cycle in the experiment of Mn40 with C_7H_8 (0.25%) and H_2O (6.67%). Times for reduction, purge and oxidation periods have been indicated by vertical dashed lines

Fig. 5 Percentage of weight loss (w/w_0) versus time in the 8^{th} cycle for the first and second step at 873 K in the TGA experiments with C_7H_8 (0.25%) and H_2O (6.67%). Ni40 (top) and Mn40 (bottom). Times for reduction, purge and oxidation periods have been indicated by vertical dashed lines

Fig. 6 Rate of mass conversion, $d\omega/dt$, as a function of mass conversion (ω) in the 8^{th} reduction step at 973 K for experiments with C_7H_8 (0.25%) and H_2O

(6.67%)

Fig. 7 Comparison of the carbon deposition percentage and solid conversion evolution in the experiments of Ni40 with C_7H_8 (2000 ppm) and no H_2O at different temperatures. Reduction time (t_R) was 4 minutes. The filled symbols correspond to the highest temperature (1073 K) and the empty ones to 873 K. The square-marked lines represent carbon deposition percentage and the circle-marked, solid conversion

Fig. 8 Comparison of the carbon deposition percentage and the solid conversion evolution in the experiments of Mn40 with C_7H_8 (600 ppm) and no H_2O at different temperatures, $t_R = 4$ minutes. The filled symbols correspond to the highest temperature (1073 K) and the empty ones to 873 K. The square-marked lines represent carbon deposition percentage and the circle-marked, solid conversion

Fig. 9 Comparison of the carbon deposition percentage and the solid conversion evolution in the experiments of Fe with C_7H_8 (1000 ppm) and no H_2O at different temperatures, $t_R = 4$ minutes. The filled symbols correspond to the highest temperature (1073 K) and the empty ones to 873 K. The square-marked lines represent carbon deposition percentage and the circle-marked, solid conversion

Fig 10. Comparison of the carbon deposition percentage and solid conversion in the experiments of Ni40 with C_7H_8 (2000 ppm) with no H_2O at 1073 K

(Figure A) and 873 K (Figure B) and different reduction times (t_R). The square-marked lines represent carbon deposition percentage and the circle-marked, solid conversion. Figure C shows carbon conversion evolution at both 1073 and 873 K. In this case, closed symbols are used for 1073 K and open symbols for 873 K

Fig 11. Comparison of the carbon deposition percentage and solid conversion in the experiments of Mn40 with C_7H_8 (600 ppm) with no H_2O at 1073 K (Figure A) and 873 K (Figure B) and different reduction times (t_R). The square-marked lines represent carbon deposition percentage and the circle-marked, solid conversion. Figure C shows carbon conversion evolution at both 1073 and 873 K. In this case, closed symbols are used for 1073 K and open symbols for 873 K

Fig 12. Comparison of the carbon deposition percentage and solid conversion in the experiments of Fe with C_7H_8 (1000 ppm) with no H_2O at 1073 K (Figure A) and different reduction times (t_R). The square-marked lines represent carbon deposition percentage and the circle-marked, solid conversion. Figure B shows carbon conversion evolution at both 1073 and 873 K. In this case, closed symbols are used for 1073 K and open symbols for 873 K

Fig 13. Comparison of the carbon deposition percentage and solid conversion in the experiments of Ni40 with C_7H_8 (2000 ppm) with different H_2O/C_7H_8 molar ratios (W) at 1073 K (Figure A) and 873 K (Figure B), $t_R = 4$ minutes. The square-marked lines represent carbon deposition percentage and the circle-marked, solid conversion. Figure C shows carbon conversion evolution

at both 1073 and 873 K. In this case, closed symbols are used for 1073 K and open symbols for 873 K

Fig 14. Comparison of the carbon deposition percentage and solid conversion in the experiments of Mn40 with C_7H_8 (600 ppm) with different H_2O/C_7H_8 molar ratios (W) at 1073 K (Figure A) and 873 K (Figure B), $t_R = 4$ minutes. The square-marked lines represent carbon deposition percentage and the circle-marked, solid conversion. Figure C shows carbon conversion evolution at both 1073 and 873 K. In this case, closed symbols are used for 1073 K and open symbols for 873 K

Fig 15. Comparison of the carbon deposition percentage and solid conversion in the experiments of Fe with C_7H_8 (1000 ppm) with different H_2O/C_7H_8 molar ratios (W) at 1073 K (Figure A), $t_R = 4$ minutes. The square-marked lines represent carbon deposition percentage and the circle-marked, solid conversion. Figure B shows carbon conversion evolution at both 1073 and 873 K. In this case, closed symbols are used for 1073 K and open symbols for 873 K

Figures

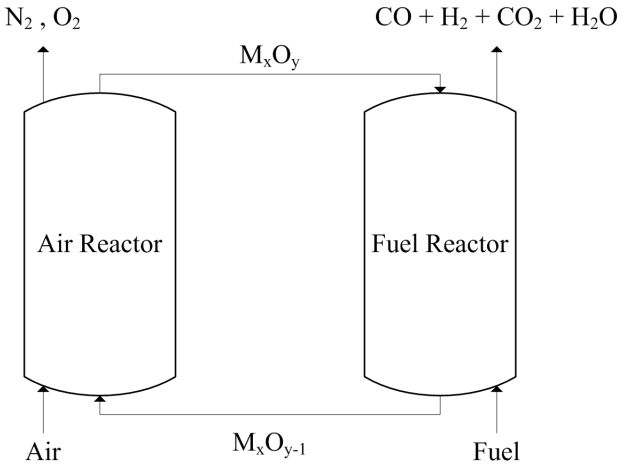

Fig. 1.

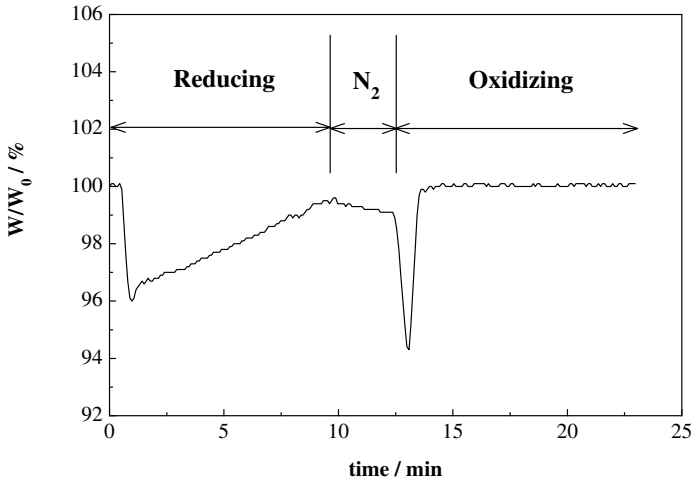
Reducing
N2
Oxidizing
W/W0 / %
time / min
106
104
102
100
98
96
94
92
0
5
10
15
20
25

Fig. 2.

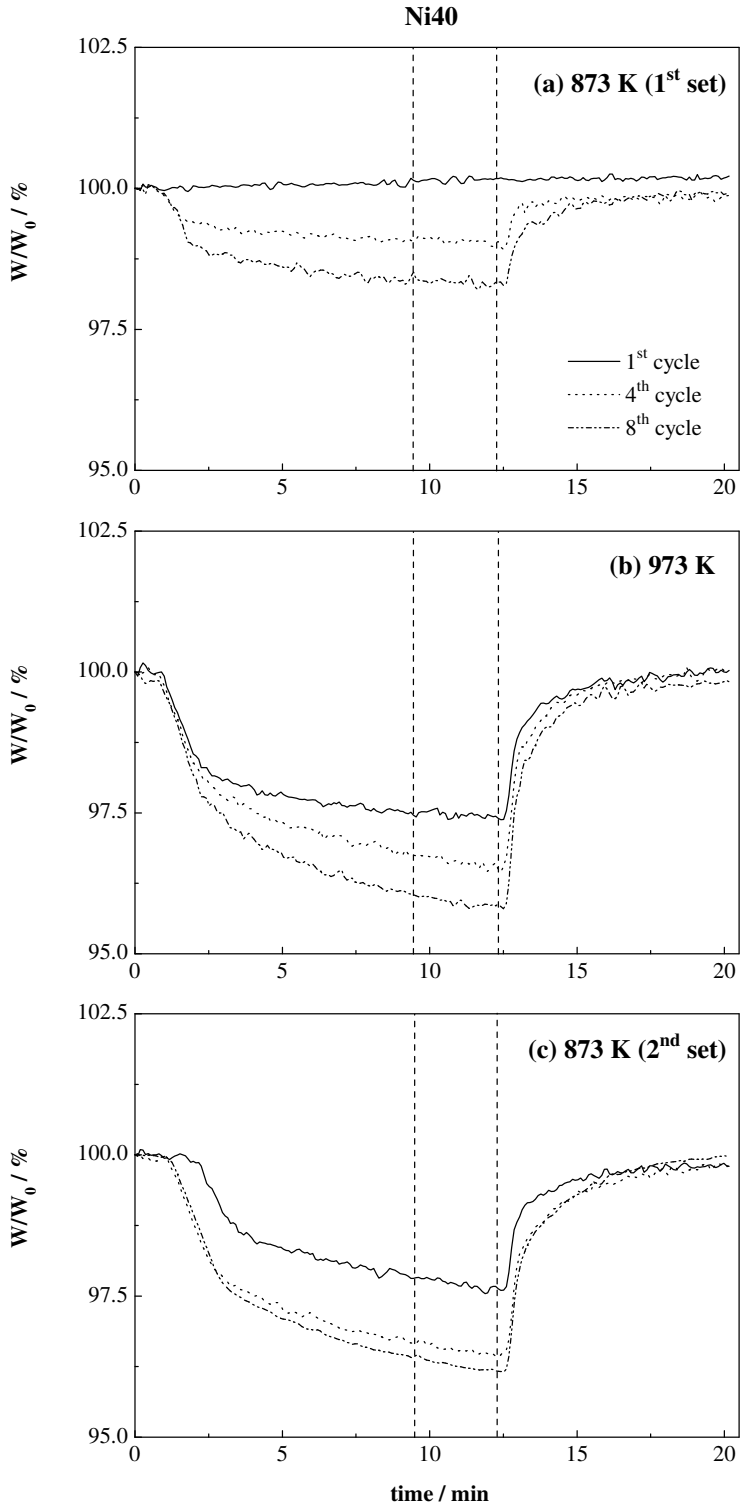
Ni40
(a) 873 K (1st set)
(b) 973 K
(c) 873 K (2nd set)
1st cycle
4th cycle
8th cycle
W/W0 / %
time / min
102.5
100.0
97.5
95.0
0
5
10
15
20

Fig. 3.

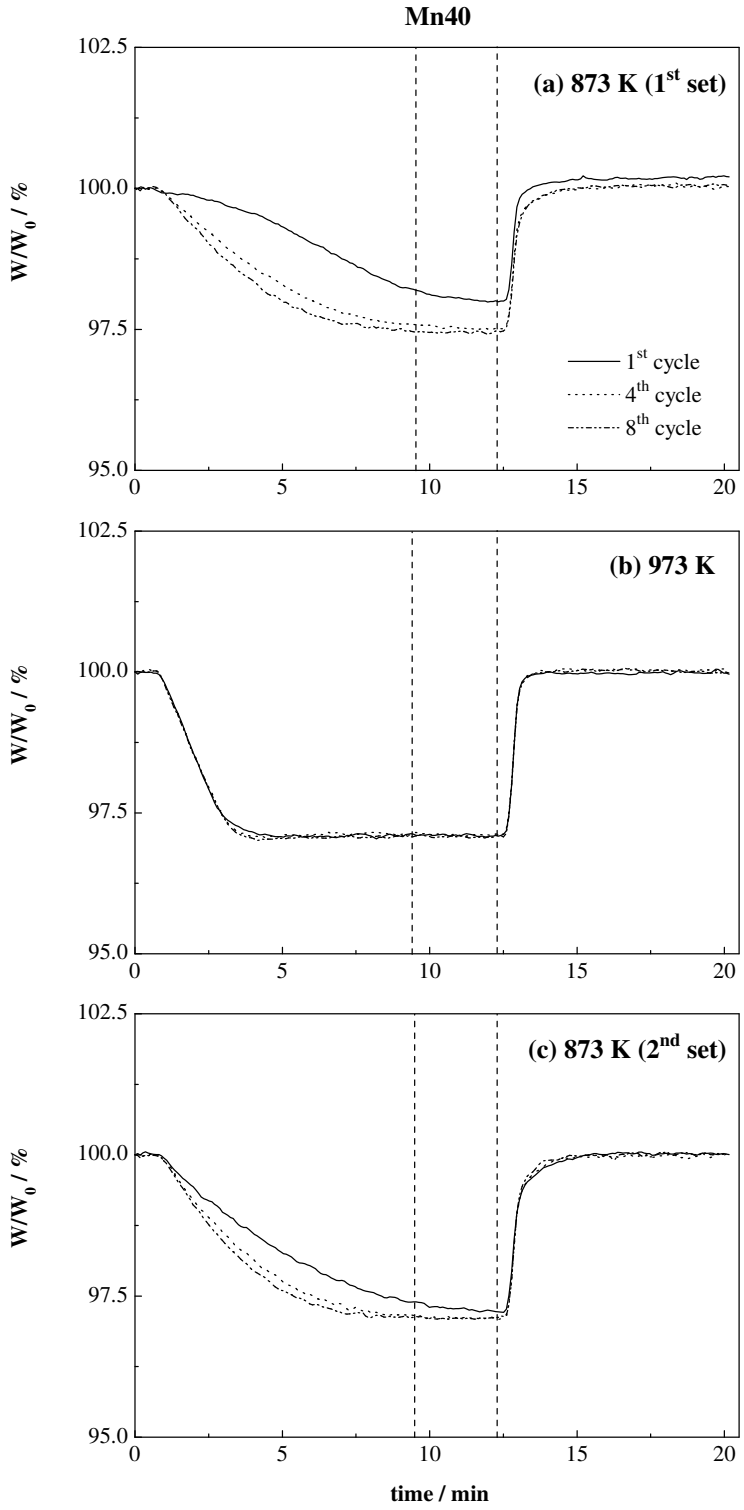
Mn40
(a) 873 K (1st set)
(b) 973 K
(c) 873 K (2nd set)
1st cycle
4th cycle
8th cycle
W/W0 / %
time / min
102.5
100.0
97.5
95.0
0
5
10
15
20

Fig. 4.

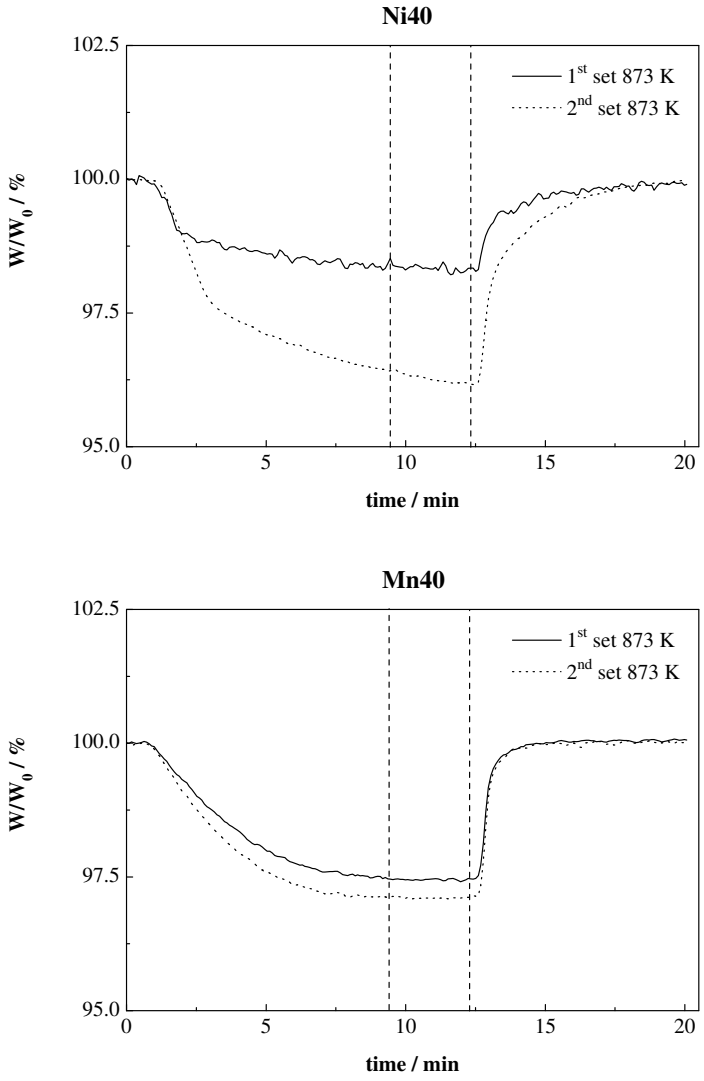
Ni40
102.5
100.0
97.5
95.0
W/W0 / %
0
5
10
15
20
time / min
1st set 873 K
2nd set 873 K
Mn40
102.5
100.0
97.5
95.0
W/W0 / %
0
5
10
15
20
time / min
1st set 873 K
2nd set 873 K

Fig. 5.

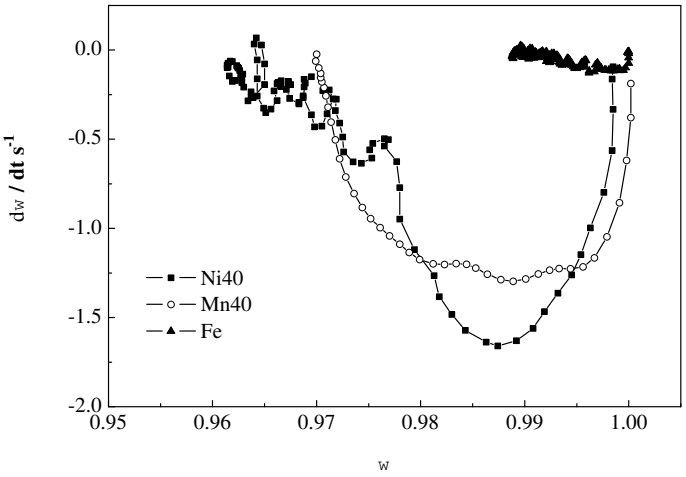

Fig. 6.

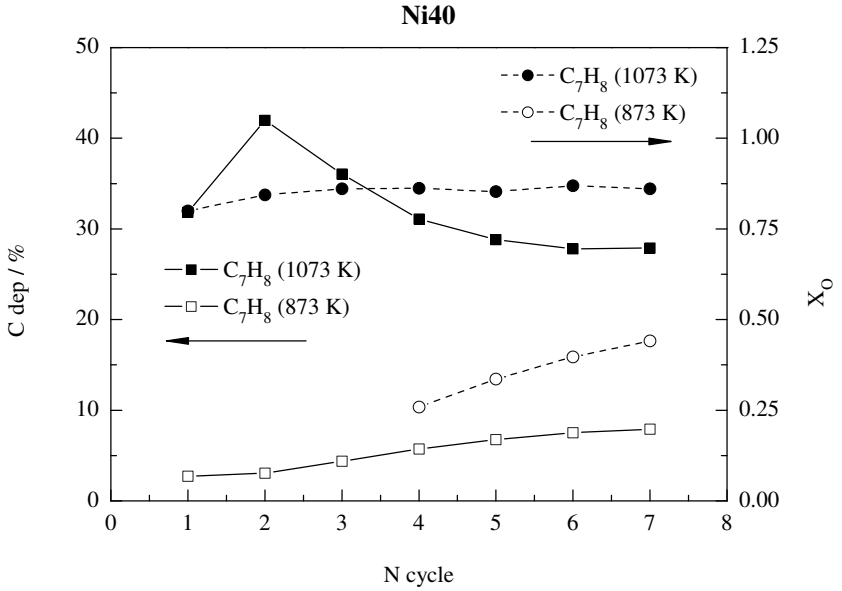
Ni40
C dep / %
X_O
N cycle
C_7H_8 (1073 K)
C_7H_8 (873 K)
C_7H_8 (1073 K)
C_7H_8 (873 K)
0
10
20
30
40
50
0.00
0.25
0.50
0.75
1.00
1.25
0
1
2
3
4
5
6
7
8

Fig. 7.

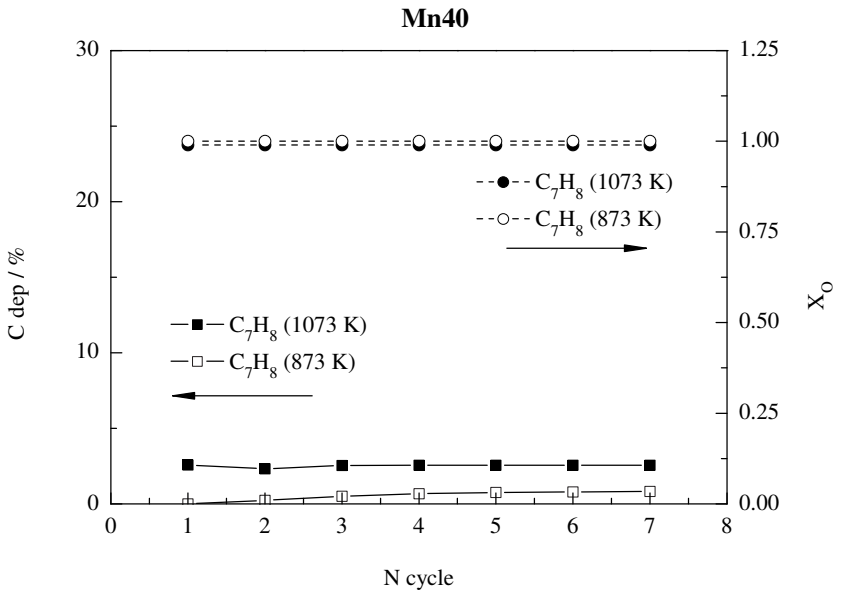
Mn40
C dep / %
X_O
N cycle
C_7H_8 (1073 K)
C_7H_8 (873 K)
C_7H_8 (1073 K)
C_7H_8 (873 K)
0
10
20
30
0.00
0.25
0.50
0.75
1.00
1.25
0
1
2
3
4
5
6
7
8

Fig. 8.

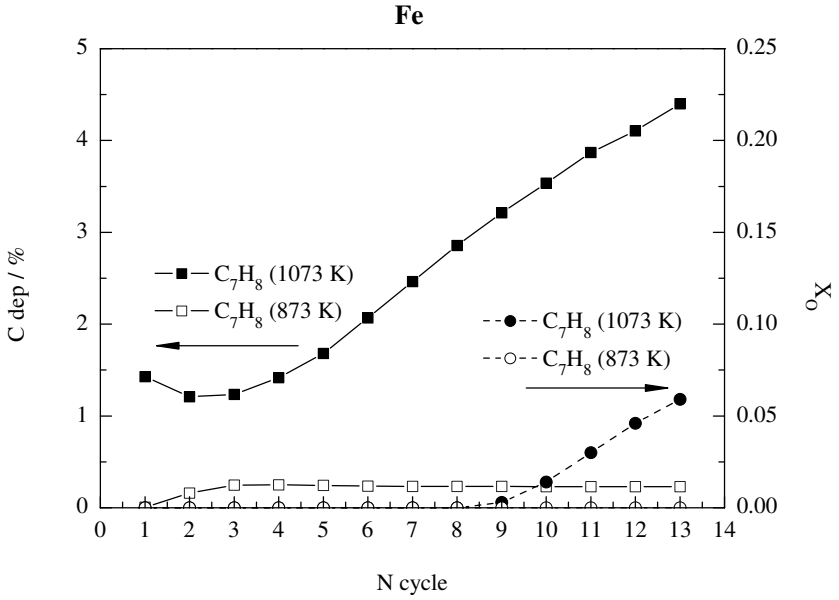
Fe
C dep / %
X_O
N cycle
C_7H_8 (1073 K)
C_7H_8 (873 K)
C_7H_8 (1073 K)
C_7H_8 (873 K)
0
1
2
3
4
5
0.00
0.05
0.10
0.15
0.20
0.25
0
1
2
3
4
5
6
7
8
9
10
11
12
13
14

Fig. 9.

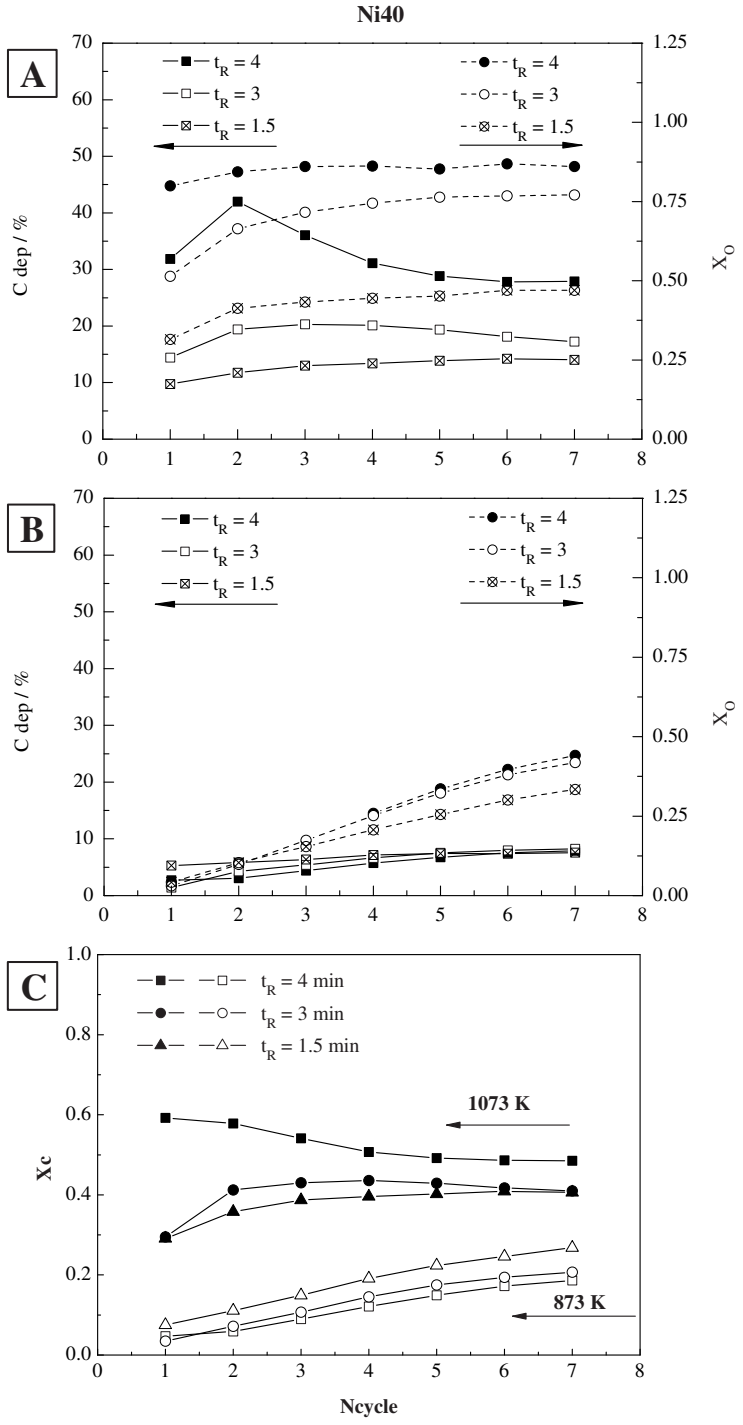
Ni40
A
B
C
C dep / %
X_O
t_R = 4
t_R = 3
t_R = 1.5
Xc
t_R = 4 min
t_R = 3 min
t_R = 1.5 min
1073 K
873 K
Ncycle

Fig. 10.

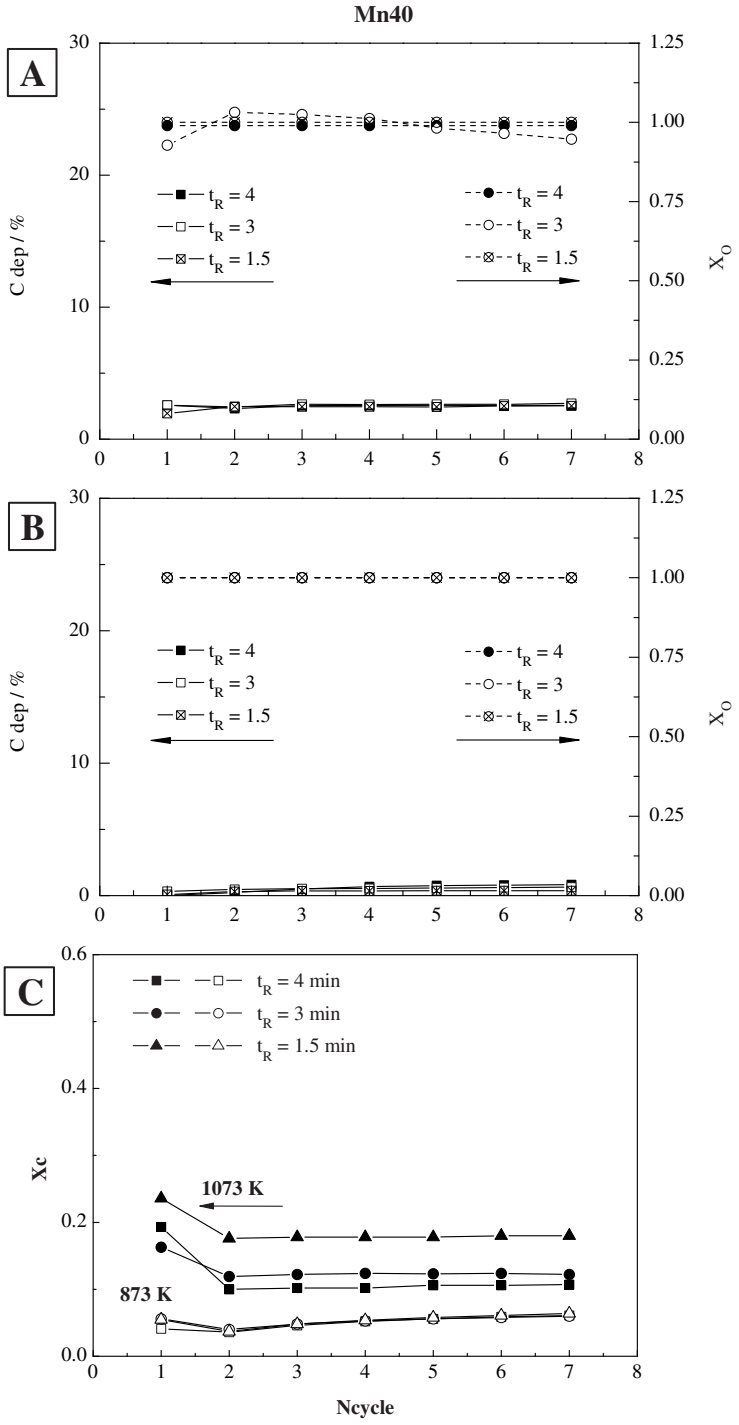
Mn40
A
B
C
C dep / %
X_O
t_R = 4
t_R = 3
t_R = 1.5
t_R = 4 min
t_R = 3 min
t_R = 1.5 min
Xc
1073 K
873 K
Ncycle

Fig. 11.

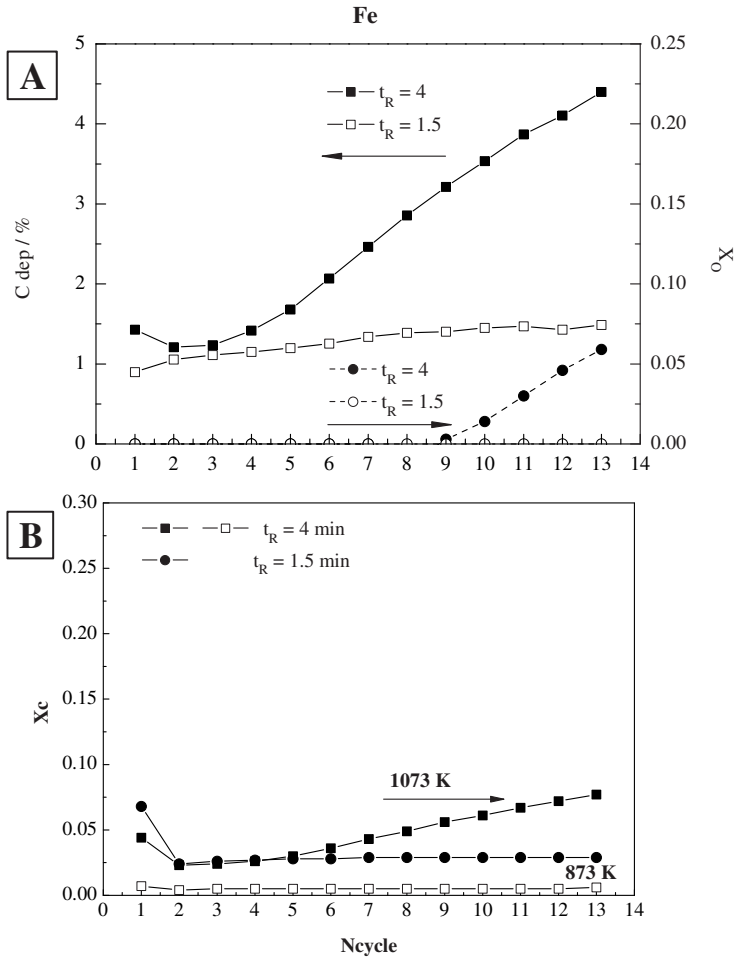

Fig. 12.

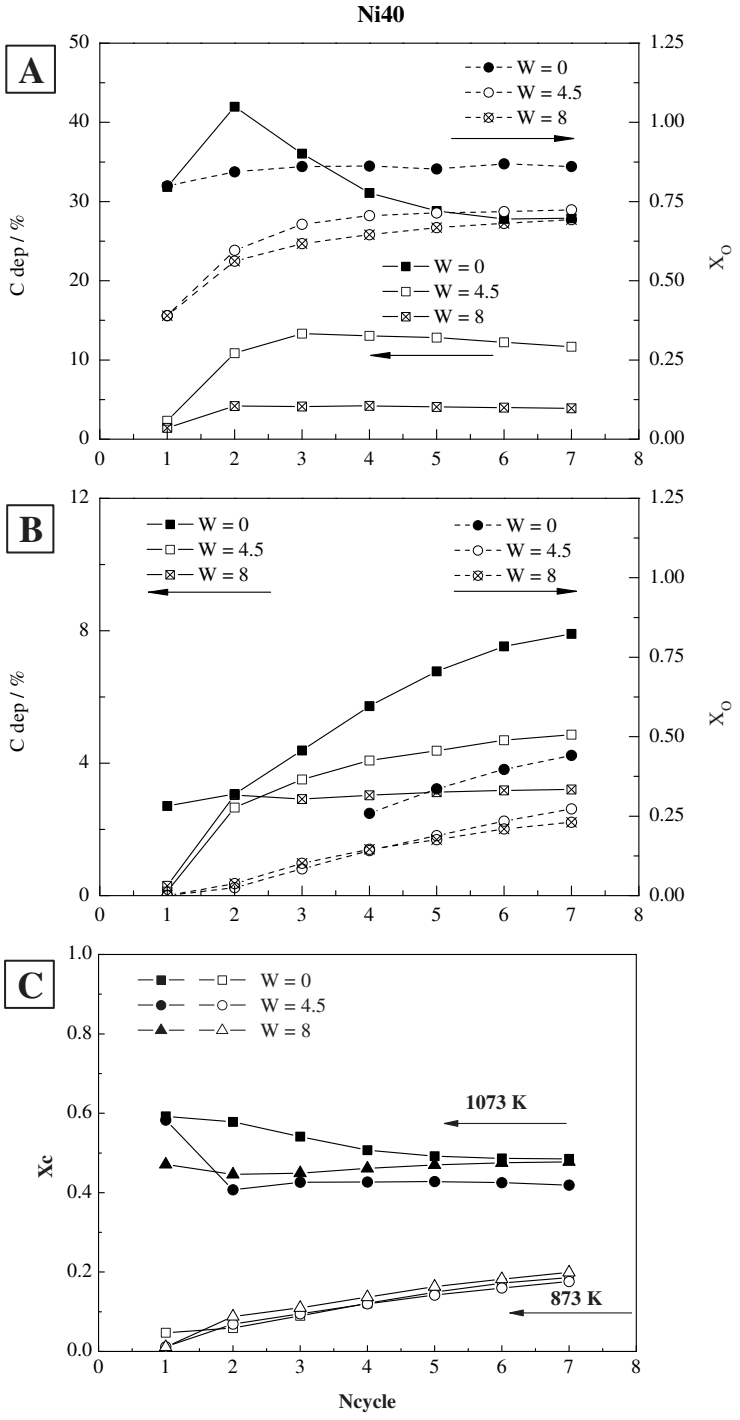

Fig. 13.

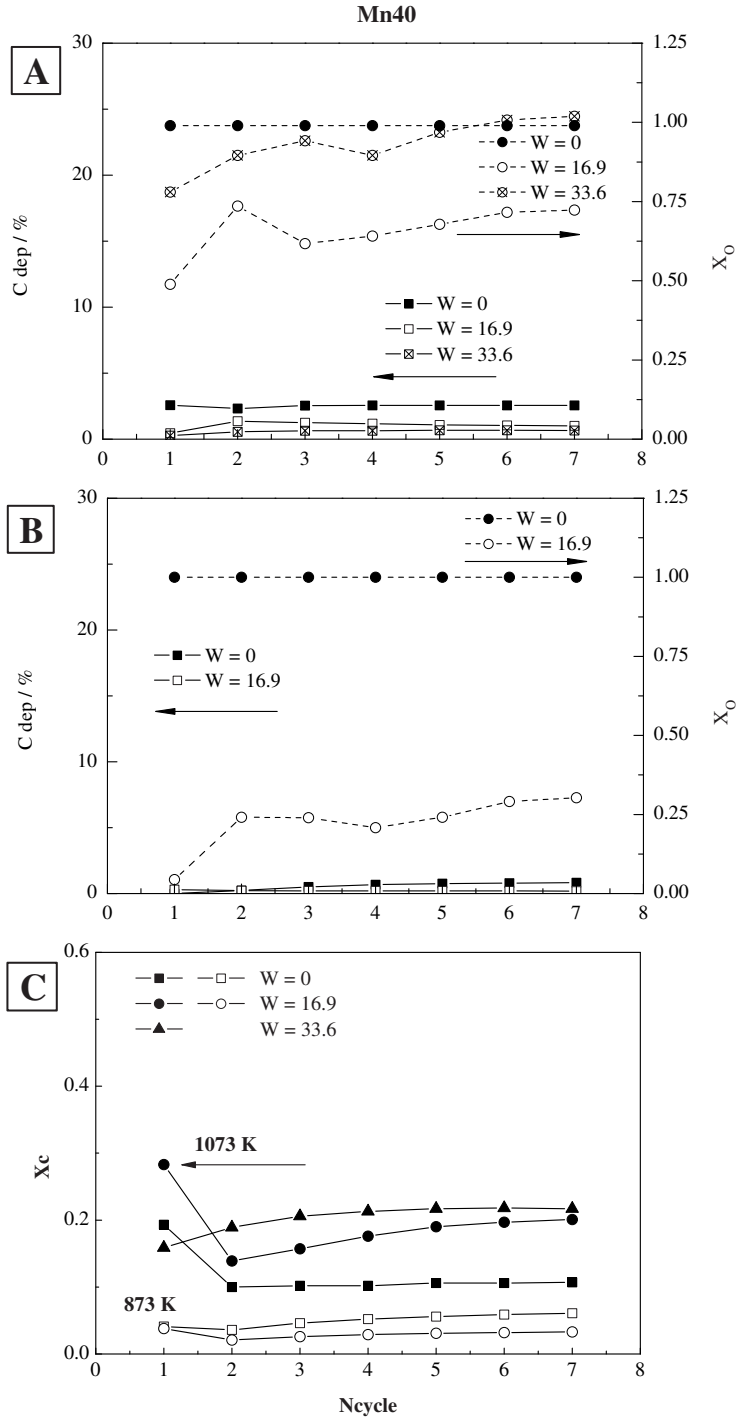
Mn40
A
C dep / %
X_O
W = 0
W = 16.9
W = 33.6
B
C dep / %
X_O
W = 0
W = 16.9
C
Xc
W = 0
W = 16.9
W = 33.6
1073 K
873 K
Ncycle

Fig. 14.

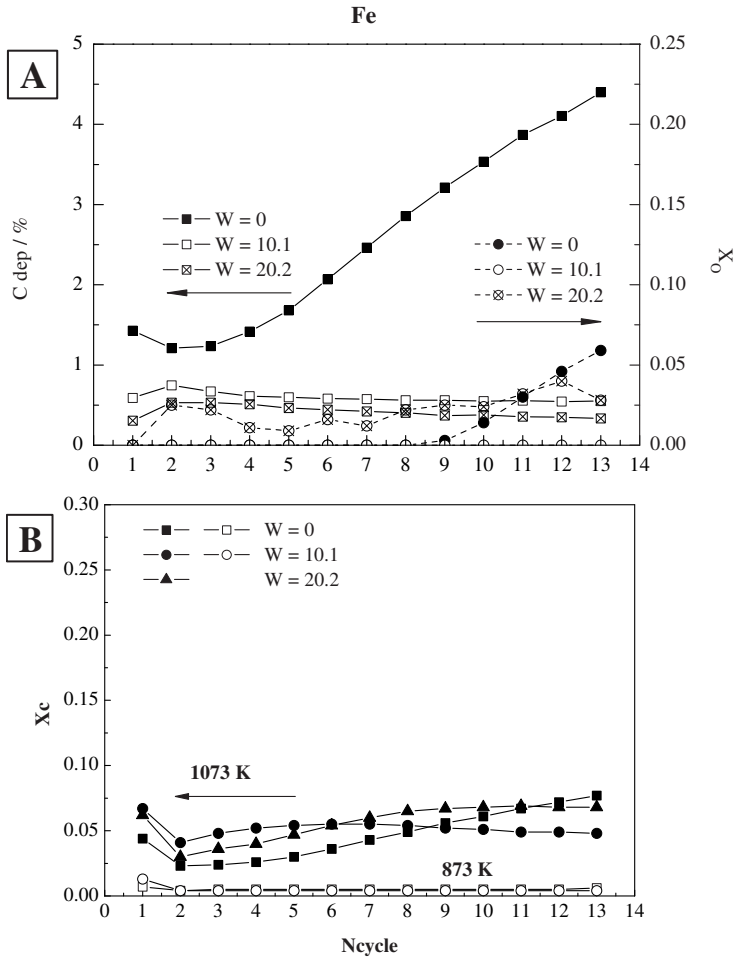
Fe
A
C dep / %
X_C
W = 0
W = 10.1
W = 20.2
W = 0
W = 10.1
W = 20.2
B
Xc
W = 0
W = 10.1
W = 20.2
1073 K
873 K
Ncycle

Fig. 15.